Quantification and Characterization of Nanoparticulate Zinc in an Urban Watershed

Shaun Bevers[1], Manuel David Montaño[2]*, Laya Rybicki[1], Thilo Hofmann[3], Frank von der Kammer[3] and James F. Ranville[1]

[1] Department of Chemistry, Colorado School of Mines, Golden, CO, United States, [2] Department of Environmental Sciences, Western Washington University, Bellingham, WA, United States, [3] Centre for Microbiology and Environmental Systems, Department of Environmental Sciences, University of Vienna, Vienna, Austria

The recent expansion in the use of nanomaterials in consumer and industrial applications has led to a growing concern over their behavior, fate, and impacts in environmental systems. However, engineered nanoparticles comprise only a small fraction of the total nanoparticle mass in aquatic systems. Human activities, particularly in urban watersheds, are increasing the population of incidental nanoparticles and are likely altering the cycling of more abundant natural nanoparticles. Accurate detection, quantification, characterization, and tracking of these different populations is important for assessing both the ecological risks of anthropogenic particles, and their impact on environmental health. The urban portion of the South Platte watershed in Denver, Colorado (United States) was sampled for zinc to identify and quantify different nanomaterial sources. Single particle ICP-QMS was employed, to provide single elemental (Zn) signals arising from particle detection events. Coupling spICP-QMS to sample pre-fractionation (sedimentation, filtration) provided some insights into Zn association with nanoparticulate, colloidal, and suspended sediment phases. Single particle ICP-TOFMS (spICP-TOFMS) provided quantification across a large atomic mass range, yielding an even more detailed characterization (elemental ratios) on a particle-by-particle basis, providing some delineation of multiple sources of particles. Across the watershed, on average, 21% of zinc mass was present as zinc-only particles with a rather uniform mean size of 40.2 nm. Zinc that was detected with one or more other elements, primarily Al, Fe, and Si, is likely to be present as heteroagglomerates or within mineral colloids. Although spICP-TOFMS provides a substantial amount of information, it is still in its early stages as an analytical technique and currently lacks the requisite sensitivity to study the smallest of nanoparticles. As this technique continues to develop, it is anticipated that this methodology can be broadly applied to study sources, behavior and effects of a disparate variety of nanoparticles from both geogenic and anthropogenic origins.

Keywords: nanoparticles, single particle ICP-MS, ICP-TOFMS, urban runoff, suspended sediments

INTRODUCTION

The combination of increasing global human populations, combined with rising urbanization have placed stress on urban watersheds through the direct influx of anthropogenic contaminants and other man-made influences (Baalousha et al., 2016; Zheng et al., 2019). The concurrent rise of impermeable surfaces in an urban environment results in greater stormwater run-off into these water bodies, (Shuster et al., 2005) carrying a variety of contaminants ranging from automotive fluids and resuspended particulate emissions, (Lamprea et al., 2018) dissolved metals, (Zuo et al., 2012) and suspended solids (Toor et al., 2017), all of which having possible deleterious effects on human and ecological health (Young et al., 2018).

The increasing development of nano-enabled consumer and industrial products has resulted in a number of potential release pathways for engineered nanoparticles (ENPs) during use and disposal (Hendren et al., 2011; Sun et al., 2017; Giese et al., 2018). In addition to intentionally ENPs, urban centers serve as a source of incidental nanoparticles (INPs) that are unintentionally produced from human-driven processes such as vehicle emissions, (Gonet and Maher, 2019) tire wear, (Sommer et al., 2018) and road dust (Yang et al., 2016). These man-made particles infiltrate urban streams via storm water, adding to the naturally occurring nanoparticulates (NNP) load present from bio- and geogenic sources (Hochella et al., 2008, Hochella et al., 2019).

One nanomaterial of particular interest is zinc oxide (ZnO). As an ENP, it is used in large quantities (10,000 tons annually circa 2012; Piccinno et al., 2012) in tire manufacture, (Milani et al., 2004) sunscreens (Herzog et al., 2002; Osmond and McCall, 2010), and paints (Kaiser et al., 2013) with the potential to leach into the environment after use. There are several sources of Zn INPs as well, primarily generated from tire wear (Councell et al., 2004), and the resuspension of road dust (Ermolin et al., 2017). While not highly toxic, zinc's effect on aquatic species has led to EPA establishing hardness-dependent water quality criteria in the few tens to hundreds µg/L range (DeForest and Van Genderen, 2012). In order to protect our urban watersheds, it is necessary to develop risk managements strategies that can effectively mitigate the influx of these potential contaminants. However, the complexity of nano-scale zinc in the environment requires the development of new sophisticated means of detection, quantification, and differentiation of the different sources of particulate zinc.

Several techniques are available to examine the elemental composition of nanoparticles in the environment. Field flow fractionation coupled to ICP-MS (FFF-ICP-MS) is one such technique that can provide elemental composition on a hydrodynamic diameter basis (Stolpe et al., 2005; Plathe et al., 2010). However, in the analysis of multi-element particles, the co-elution of particle populations makes it difficult to discern between particles containing many elements, and distinct populations of similar sizes eluting simultaneously. In order to quantify particle composition on an individual particle basis, single particle ICP-MS (spICP-MS) has a widely demonstrated utility in the analysis of natural waters for ENPs (Furtado et al., 2014; Gondikas et al., 2014) and NNPs (Praetorius et al., 2017; Gondikas et al., 2018). In a study examining TiO$_2$ ENP release from sunscreens, spICP-MS was utilized to demonstrate an increase in particulate Ti from anthropogenic activity (Reed et al., 2017). Hadioui et al. (2015) used ICP-quadrupole-MS (ICP-QMS) coupled with ion exchange chromatography to measure ZnO nanoparticles in the presence of high dissolved Zn backgrounds. Expanding upon this work, Fréchette-Viens et al. (2019) employed a high-resolution, ICP-sector-field-MS instrument to push the size detection limits of ZnO nanoparticles in surface waters while noting the presence of larger heteroaggregate particles containing small amount of Zn. Nevertheless, these studies also highlight a fundamental weakness of quadrupole mass analyzers in their inability to monitor multiple ions simultaneously. Though some studies have shown the potential to monitor two or more elements in a given particle event, (Montaño et al., 2014; Heringer and Ranville, 2018) to accurately characterize the source of nanoparticulate Zn requires a means of analyzing multiple elements simultaneously. In recent years, commercially available ICP-time-of-flight-mass spectrometry (ICP-TOFMS) has shown the potential to significantly augment the utility of single particle analysis. The intrinsic nature of time-of-flight mass analysis permits the quasi-simultaneous detection of a wide mass range on microsecond time scales, the duration being bound to the extraction frequency. Typical acquisition times (33-46 µs; Gschwind et al., 2011; Borovinskaya et al., 2013; Hendriks et al., 2017) are on the same order as the nanoparticle detection events (500 µs) (Olesik and Gray, 2012). Recent studies have demonstrated its utility in characterizing a variety of nanomaterials ranging from simple core-shell ENPs (Naasz et al., 2018) and multi-element steel NPs (Hegetschweiler et al., 2018) to more complex atmospheric nanoparticulates (Erhardt et al., 2019). Given this capability, ascertaining the sources of NPs may be possible by monitoring the respective elemental or isotopic ratios on a particle-by-particle basis (Praetorius et al., 2017; Montaño et al., 2019).

In this study we demonstrate a multi-method approach for detecting and quantifying Zn NPs in the portion of the South Platte Watershed that encompasses Denver, CO (United States). Water samples were taken from multiple tributaries and the main stem of the South Platte River in mid-July 2018 within 2 days of a large storm event that significantly increased stream flow. Settling and filtration were used to separate different size fractions of particulate zinc, which were then quantified by spICP-QMS. Analysis by spICP-TOFMS provided particle-by-particle elemental associations of zinc to investigate the sources of Zn NPs across the watershed.

MATERIALS AND METHODS

Study Location

The urban reaches of the South Platte River, the primary water source for Denver (CO, United States), as well as several of
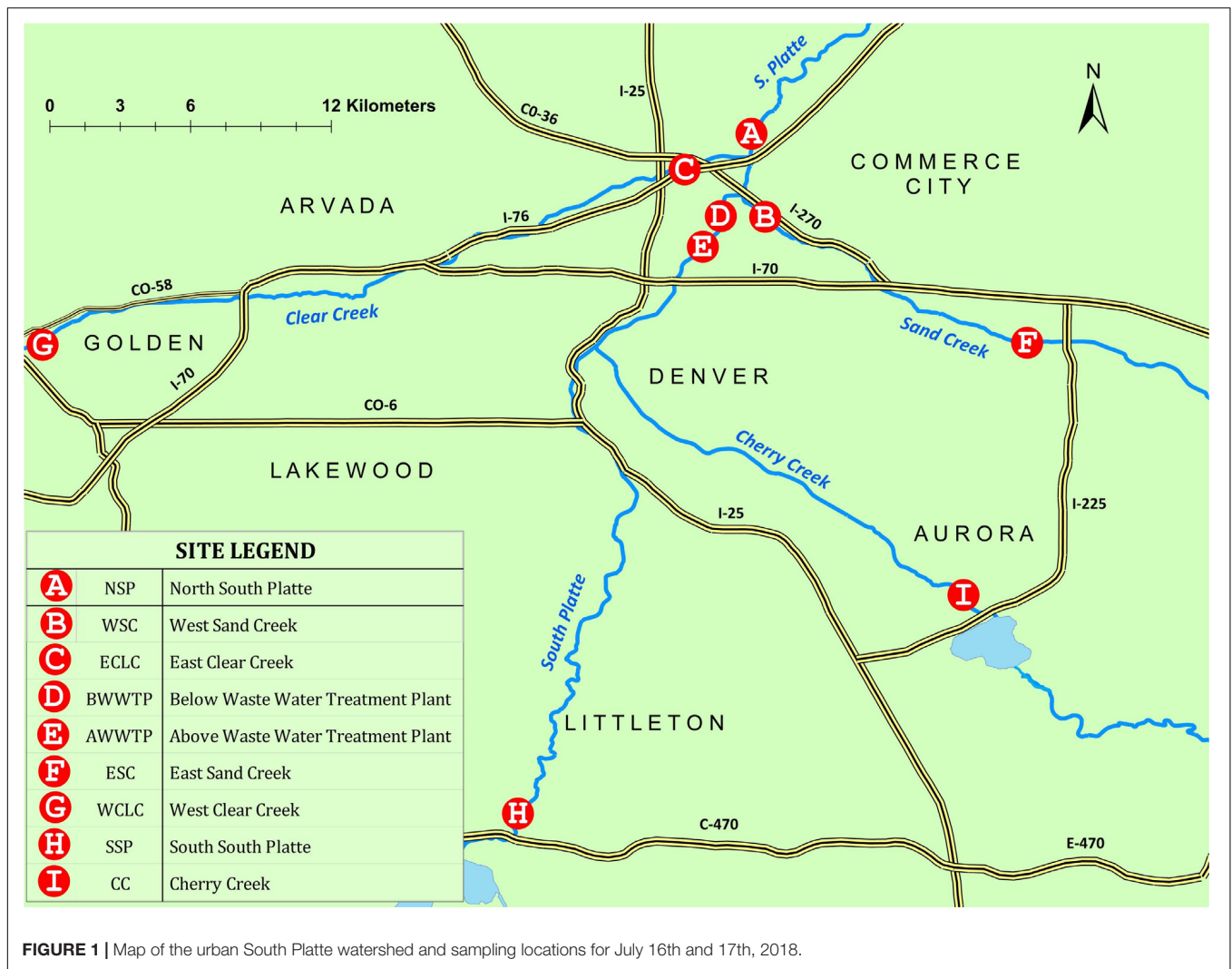
FIGURE 1 | Map of the urban South Platte watershed and sampling locations for July 16th and 17th, 2018.

its tributaries were examined (**Figure 1**). The South Platte River enters the metro area from the southwest corner and exits north of the city. Major tributaries that feed the South Platte River within the Denver metro area include Clear Creek (ClC), Cherry Creek (CC), and Sand Creek (SC). Chatfield Reservoir is the only significant impoundment on the South Platte River itself and it intercepts flow emanating from the mountains upstream of the study site. Cherry Creek Reservoir is the other significant impoundment in the watershed, existing on the Cherry Creek tributary also upstream of the sampling site. Streamflow throughout the basin is low during fall and winter months. Flow increases beginning in April and peaks in the months of June and July as a result of mountain snow melt. Water impoundment and release from the aforementioned reservoirs can have significant effects on streamflow along with agricultural diversion through numerous ditches during the growing season. Annual precipitation in the metro area ranges between 180–380 mm per year, which mostly falls during April to September. Notably, much of the summer precipitation occurs as brief-duration thunderstorms, resulting in short-term elevated stream flow. Sampling was timed to capture urban runoff following one such event in 2018.

Field Sampling

Sampling was performed on July 16th and 17th, 2018 following a rainfall event on July 14th–15th. Rainfall was not uniform across the basin and resulted in streamflow increases that varied among the sampling locations (hydrographs provided in ESI **Figure 1**). On July 16th five sites were sampled (**Figure 1**); three sites examined the confluence between the South Platte River downstream Denver (flow to the north), Clear Creek (flow from the west), and Sand Creek (flow from the east). Two samples were also taken from the South Platte River at points approximately 500 m upstream and downstream of the Robert W. Hite wastewater treatment plant, the largest such facility in Denver. Locations are labeled as: WSC (West Sand Creek), EClC (East Clear Creek), NSP (North South Platte), AWTTP (South Platte above the wastewater treatment plant), and BWTTP (South Platte below the wastewater treatment plant). To examine tributary inputs from outside the central urban area, sampling on

July 17th occurred at locations labeled ESC (East Sand Creek), WClC (West Clear Creek), SSP (South South Platte), and CC (Cherry Creek). Both EClC and NSP were also resampled on this date (**Figure 1**).

Grab samples were collected by submerging polyethylene bottles (1 L) approximately 10 cm or more below the surface, at a point at least 0.5 meter from the streambank. Bottles were filled and emptied three times to rinse the virgin bottles prior to collecting the sample. Subsamples were taken for chemical analysis in the laboratory at Colorado School of Mines. The remaining sample was stored at 4°C until further processing and single particle ICP-MS analysis.

Laboratory Analysis/Preparation

Subsamples (10 ml) were subjected to a modification of the EPA Total Recoverable (TR) Method, EPA 200.2 (United States Environmental Protection Agency [EPA], 1994). To accommodate our small-footprint digestion equipment, the method was modified by reducing the sample and acid volumes by a factor of 10. All other aspects of EPA 200.2 remained unchanged. All samples were shaken prior to subsampling. Cation concentrations were determined by ICP-OES (PerkinElmer Optima 7300 DV), the operational details and QA procedures being provided in ESI. Major anions (Cl and SO_4) were measured by ion chromatography (Dionex: ThermoFisher, ICS-900, Waltham, MA, United States). Turbidity measurements were made using a Hach DR 890 meter (HACH Method 8237), and results reported in formazin absorbance units (FAU). Results for metals, anions and turbidity are reported in **Table 1**.

Single Element, Single Particle ICP-QMS Analysis

Single particle ICP-QMS analysis was performed using an ICP-quadrupole mass spectrometer (NexION 300 D, Perkin Elmer, Waltham, MA, United States). For single particle analysis, the transport efficiency (TE) was determined using the mass-based method as described by Pace et al. (2011) and reported in

Supplementary Table S1. A 60 nm Au nanoparticle (NIST SRM 8013, citrate-stabilized, mean size of 56.0 ± 0.5 nm by TEM) was used as a known mass standard. Dissolved standards of 0 to 100 µg/L Au [SPEX CertiPrep in 2% (v/v) hydrochloric acid] and Zn [SPEX CertiPrep in 2% (v/v) nitric acid] were prepared using nitric acid (Fisher Scientific, Optima grade, 32-35%) and were diluted in Milli-Q water (18.2 MΩ-cm, Barnstead International) on the day of each analysis. All unfiltered samples and Au NP standards were sonicated in a sonic bath for 5 min prior to analysis. ^{197}Au or ^{64}Zn were analyzed using a dwell time of 100 µs, no settling time, sample flow rate = 0.3 ml/min, a total data collection time of 60 s, and a very short detector dead time (35 ns) between readings. Data acquisition and data processing were performed using the Syngistix^{TM} Nano Application Module (PerkinElmer). TE determination is built into the software and is calculated in order to determine NP mass (from which size is computed) and the number concentration. Particle events were identified as ICP-MS responses that were deemed to above the threshold intensity, which was determined in real-time using the average background plus 3σ (Pace et al., 2011). The particle number concentration is computed from the number of NP events detected after adjustment for the sample flow rate and TE. In addition to particle analysis, data collected by spICP-QMS was integrated over the entire 60 s analysis and, through use of the calibration curves, the mass concentration of Zn (µg/L) was determined.

Additional Sampling Processing for spICP-QMS

Samples were also filtered through a 0.02 µm filter (Whatman Anotop) prior to spICP-QMS analysis to obtain an estimate of the dissolved elemental concentration (µg/L). Filtered samples also provided a means of evaluating the spICP-QMS baseline obtained for non-filtered samples. This is often assumed to represent the dissolved element mass concentration (µg/L). A crucial parameter in sizing nanomaterials by spICP-MS is the selection of particle composition (i.e., element mass fraction and density), and geometry. As a quadrupole mass analyzer is only capable of

TABLE 1 | Bulk water chemistry data for sample sites used in this study.

Sampling date	Turbidity (FAU)	Total recoverable metals (mg/L)					Anions (mg/L)		spICP-MS (µg/L)	
		Al	Si	Fe	Mn	Zn	Cl	SO$_4$	Zn	% recovery
16-Jul										
NSP	50	1.39	7.01	1.57	0.20	0.043	60	77	11.5	27
WSC	170	7.57	20.64	6.86	0.38	0.068	65	171	13.9	20
EClC	31	1.03	5.72	1.33	0.19	0.049	49	61	13.3	27
BWWTP	27	1.20	6.54	1.25	0.15	0.032	69	81	9.2	29
AWWTP	32	1.27	6.54	1.31	0.16	0.026	61	69	6.3	24
17-Jul										
NSP	29	1.00	6.87	0.99	0.20	0.050	93	151	13.7	27
ESC	258	10.67	27.88	9.03	0.35	0.072	42	196	19.9	28
EClC	13	0.16	4.10	0.31	0.19	0.022	75	86	8.4	38
WClC	7	0.17	3.20	0.34	0.05	0.061	14	35	23.2	38
SSP	19	0.61	3.79	0.62	0.40	0.009	67	73	1.8	20
CC	7	0.46	9.29	0.41	0.27	0.004	189	177	1.2	29

selecting for one mass-to-charge ratio at a time, it is necessary to utilize other means to approximate the values needed for particle sizing. To provide this additional information on the Zn-containing particles, each non-filtered sample was gently agitated and then subjected to settling in a 15 ml centrifuge tube (VWR, Falcon brand). Sampling from the upper 2 cm after 70 min provided a size separation at approximately 4.5 μm, assuming a spherical particle with a density of 2.65 g/cm^3, typical of sediment minerals. Using ZnO density 5.61 g/cm^3 gives an approximate size cutoff of 2.5 μm. Comparison of the observed changes in NP mass (size) and integrated concentration (number/ml and μg/L), to that predicted assuming the Zn was present as either ZnO or associated with sediment particles, provides insight into Zn form/mineralogy.

Multi Element, Single Particle ICP-TOFMS Analysis

Unfiltered samples were examined by multi-element analysis using single particle ICP- time-of-flight mass spectrometry (spICP-TOFMS) at the University of Vienna. Data were collected using an icpTOF 2R (TOFWERK AG, Thun, Switzerland). The ICP-TOF has a mass-resolving power of 6000 FWHM and a TOF extraction frequency of 46 kHz, measuring a majority of the atomic mass range (7–250 m/z$^+$). The operation of the ICP-TOF utilizes a notch filter, which allows for the attenuation of up to four chosen masses, typically chosen for their abundance, which can lead to signal suppression of ions of interest. In this case, ^{40}Ar$^+$, ^{16}O$_2^+$, ^{35}Cl$^+$, and ^{1}H$^+$ were chosen. To improve the signal-to-noise of ^{56}Fe$^+$ and ^{28}Si$^+$, both of which have isobaric interferences in ^{40}Ar^{16}O$^+$ and ^{14}N$_2^+$, respectively, a 7% H$_2$/He mixture was used for a collision gas. The flow parameters of this gas were optimized before analysis for maximum sensitivity. Dissolved calibration solutions were prepared from ESI stock solution of dissolved metals (Al, Si, Fe, Cu, Ti, Zn, Pb, Cd, Cu, Nd, Ni, and Au), analyzed prior to each sample run, with a continuing check verification standard (CCV) every 10 samples to account for any drift in instrument sensitivity. Additional and typical operating parameters are listed in supporting information (**Supplementary Table S1**). A 100 nm gold nanoparticle (BBI solution) was used as a known mass standard for obtaining TE. Due to limitations on data transfer from the data acquisition system to the laboratory computer, a 3 ms dwell time was used, despite the much shorter mass sweep time. To avoid particle coincidence for this long dwell time, a 1000$\times$ dilution of the samples was required. This was not required for the spICP-QMS analysis.

The raw mass spectrum data were initially processed using TofWare (TOFWERK AG, Thun, Switzerland) which allowed for peak integration after initial subtraction of the spectral baseline. The resulting data was then processed via a custom Python script which performed calibration and spectral correction of the data. The script also then processed the single particle data according to the previously established methodology (Pace et al., 2011; Laborda et al., 2014; Montano et al., 2016), which was similar to that used for spICP-QMS analysis. The subsequent data output

resulted in a compiled list of particle events with time and their associated masses, which can then be converted into mass and size according to single particle theory.

RESULTS

Bulk Water Chemistry

Total recoverable mass concentrations (μg/L) for those elements that were also examined by spICP-MS are given in **Table 1**, with major cation concentrations provided in ESI. Although TR aggressively digests suspended sediments, in most cases particulate matter remained after the digestion and was removed by filtration (0.45 μm, nylon, GEI). Samples from Sand Creek contained considerably more suspended sediment than those from other sites. Chloride and sulfate were the major anions measured (**Table 1**). Alkalinity, representing another possible major anion, was not measured. Turbidity (**Table 1**) was used as a surrogate for suspended sediment concentration.

Single Element, spICP-QMS Results

Data collected for the unfiltered sample using spICP-QMS was integrated over the entire 60 s analysis to determine the mass concentration of Zn (**Table 1**). The number of particles measured in the raw samples (60 s analysis time) were, with one exception, always greater than 1000, and in most cases greater than 2000 (**Figure 2A**). Accounting for flow rate and transport efficiency resulted in calculated particle number concentrations for most samples of between 7500 and 170,000 particles/mL (**Table 2**). Integration of the particle-generated ^{64}Zn pulses yields a range of 0.5 to 9 femtograms for the number-weighted, geometric mean of the Zn mass contained in each particle (**Figure 2B**).

Analysis of unfiltered samples by spICP-QMS resulted in a series of pulses (representing NPs) over an elevated background (**Figure 3A**). We have applied a methodology that defines the Zn distribution as being composed of resolved, unresolved, and dissolved fractions. Resolved nanoparticulate Zn (RP) represents particles that have sufficient Zn content to be discriminated from the baseline signal when using the Syngistix software. In spICP-MS analysis, the baseline elemental signal is often considered to approximate the dissolved metal concentration (Montaño et al., 2014). Analysis of the 0.02 μm membrane-filtered sample gives a more direct approximation of dissolved Zn (**Figure 3B**) by removing a majority of particulate Zn, although smaller NPs could be present in this fraction. This pore size is well below the size detection limit of the spICP-QMS (approximately 50 nm as ZnO; Lee et al., 2014) and thus would not contain observable individual NPs. In this study, we also define an unresolved nanoparticle fraction (URNP) as the difference between the Zn baseline concentration in the raw sample $[(Zn)_{Raw,Diss.Baseline}]$ minus the 0.02 μm filtered sample $[(Zn)_{0.02\,\mu m,Diss.Baseline}]$.

$$[Zn]_{URNP}\,(\mu g/L) = [Zn]_{Raw,Diss.Baseline} - [Zn]_{0.02\,\mu m,Diss.Baseline}$$
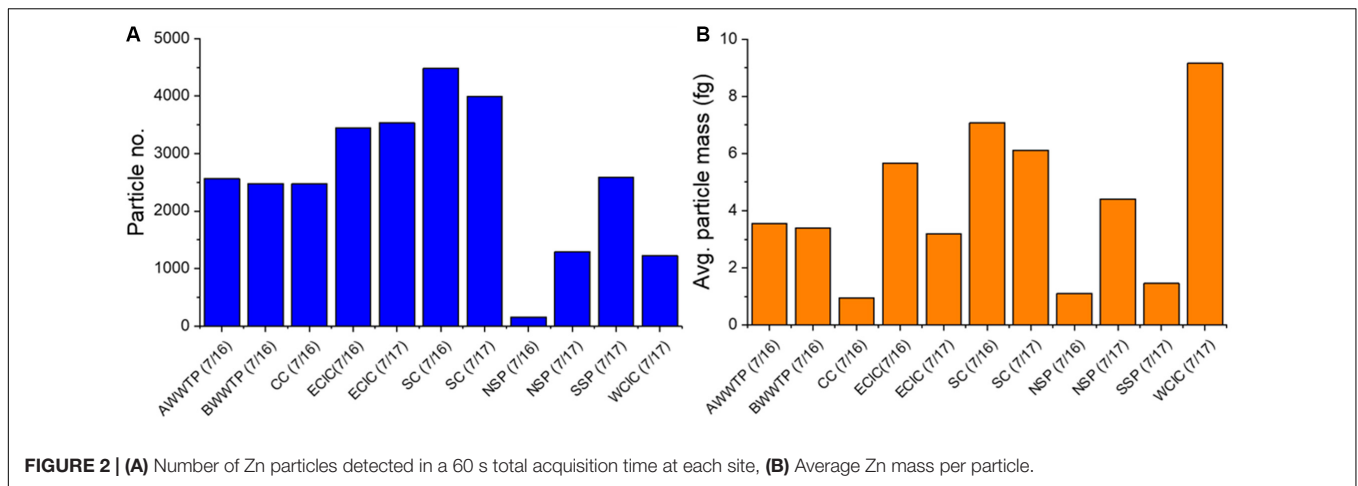
(1)

FIGURE 2 | (A) Number of Zn particles detected in a 60 s total acquisition time at each site, (B) Average Zn mass per particle.

TABLE 2 | spICP-MS quantification of Zn particle and dissolved fractions at the various sample sites used in this study.

Sampling date	Particle conc. (#/L)		Average diameter (ZnO eq.)		Background dissolved Zn (ppb)		
	Raw	Settled	Raw	Settled	Raw	Settled	0.02 filtered
16-Jul							
NSP	7.6E+03	1.4E+05	67	96	11.2	8.4	3.9
WSC	2.2E+03	2.4E+05	124	95	13.9	7.2	0.9
ECIC	1.7E+05	1.2E+05	115	102	13.3	10.1	4.0
BWWTP	1.2E+05	4.5E+04	97	91	9.2	7.9	5.2
AWWTP	1.3E+05	8.6E+04	98	86	6.3	4.6	1.7
17-Jul							
NSP	6.4E+04	1.4E+05	106	96	13.7	8.2	1.6
ESC	2.0E+05	1.9E+05	118	107	19.9	13.5	0.3
ECIC	1.7E+05	1.5E+05	95	90	8.4	6.6	5.2
WCIC	6.0E+05	3.8E+04	135	132	23.2	18.6	1.9
SSP	1.3E+05	1.1E+05	73	66	1.8	0.3	0.2
CC	1.2E+05	1.0E+05	63	62	1.2	0.8	0.4

Values reported for both raw and settled samples.

For the example shown (**Figure 3**), the peaks before filtration (**Figure 3A**) represent the RP fraction. The baseline in the raw and the 0.02 μm filtered samples (**Figure 3B**) give "dissolved" Zn concentrations of 6.1 μg/L and of 0.8 μg/L, respectively. Subsequently the difference of these two values give the URNP Zn concentration of 5.3 μg/L. The distribution in the Zn mass concentration of these three fractions across the watershed is shown in **Figure 4** (**Supplementary Table S3**).
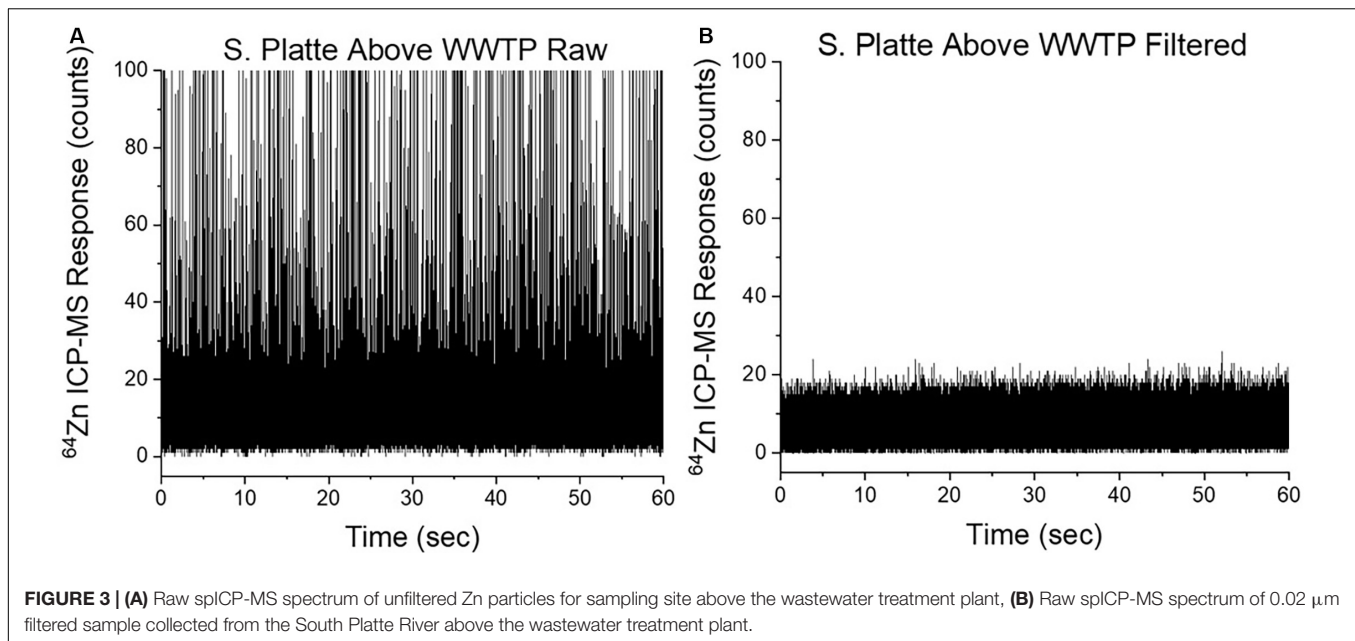
Settling experiments were an attempt to examine Zn that might be present as ZnO (density = 5.61 g/cm^3) and as zinc-associated with mineral matter (density = 2.65 g/cm^3). Integration of Zn counts obtained by spICP-QMS for the settling experiments provided the mass concentrations of Zn (μg/L) in each of three fractions that were defined as particulate (i.e., subject to settling), colloidal (i.e., non-settleable), and dissolved (0.02 μm filtrate). Subtraction of the integrated Zn counts measured after settling from that of the raw sample was used to compute the particulate fraction. Likewise, subtraction of the integrated Zn counts for the 0.02 μm filtered sample from the counts for the sample after settling yields a colloidal fraction.

Figure 5A provides an example of this categorization for the mass concentration (μg/L) as well as the effect on the mean particle size determination, details provided in subsequent discussion of particle characterization. The distribution of these fractions across the watershed is shown in **Figure 6** (**Supplementary Table S4**).

Multiple Element, spICP-TOFMS Results

Results of the spICP-TOFMS analysis of samples collected from across the basin are presented as pie charts (**Figure 7**) with orange to represent particles that contained no detectable element other than Zn and blue as particles containing elements in addition to Zn, with Fe, Mn, Al, and Si being the other detected elements. The numerical values of detected events of ^{64}Zn in these two classes are also displayed in **Figure 7**.

Zn nanoparticles detected across all sites are represented in **Figure 8A** by the percent mass of Zn of which they are composed. Particles were detected primarily in two categories: those composed of high (>95%) and very low (<5%) proportions of Zn mass. With ICP-TOFMS we can use the observed elemental

FIGURE 3 | (A) Raw spICP-MS spectrum of unfiltered Zn particles for sampling site above the wastewater treatment plant, **(B)** Raw spICP-MS spectrum of 0.02 μm filtered sample collected from the South Platte River above the wastewater treatment plant.

associations to make better estimates of overall particle size. Although the mineralogy is not known, it is a reasonable assumption that the Zn-only particles (>95%) present in fully oxygenated surface waters are ZnO. To approximate the size of the particles containing multiple elements (<5% and 5–95%) we converted the elements to their oxides (i.e., Al_2O_3, SiO_2, MnO_2, Fe_2O_3, and ZnO), calculated a volume for each oxide from the mass and density, summed the volumes of all oxides present in the particle and computed an average spherical size (**Figure 8B**). To examine spatial differences, the average and variation (box and whiskers plots) of particle diameters from each sample location were computed (**Figure 9**). Diameters were calculated assuming all Zn is present as ZnO (**Figure 9A**), as would be done for single element spICP-MS, and using the sum of the metal oxide mass, obtained by spICP-TOFMS (**Figure 9B**).

DISCUSSION

General Water Chemistry
Total Recoverable Metals and Turbidity Across Watershed
The TR metals concentrations (**Table 1**) varied little across the watershed, but for two notable exceptions. Elevated levels of Si, Al and Fe (2–5×) were found in samples from both Sand Creek sites as compared to all other sampling sites. This observation correlated with a higher turbidity measured at these two sites (East, 258 FAU; West, and 170 FAU), suggesting that these elements are present largely as part of the total suspended sediments. TR concentrations of each metal show strong correlations ($0.94 < R^2$) with turbidity (ESI **Figure 2**), consistent with their abundance in earth materials and their low solubility in neutral waters. TR Zn shows a weaker relationship to turbidity, but there are several observations that bear further

examination. The West Clear Creek site has a high TR Zn concentration (0.068 mg/L) but a low turbidity (7 FAU), which could be attributed to dissolved Zn from mining inputs upstream of the watershed. Most of the urban waters have a moderate correlation ($R^2 = 0.66$) between these two parameters, if both sand creek sites are also excluded. These two sites show a combination of high TR Zn and turbidity, but the ratio of these two parameters is lower than for the other urban sites. This observation suggests that the high total suspended solids in Sand creek contains some amount of Zn, but not at the level seen in the other urban waters. The severe rainfall event on July 15th, 2018 (ESI **Figure 1**), which was more evident on the east side of the urban area, most likely mobilized sediment leading to the high measured turbidity. Although not investigated, we note that the central urban sites appear to have the higher levels of both sulfate and chloride, likely indicating generally poorer water quality than WClC, a less urbanized upstream site.

Settling Results for Mass Concentrations (Particulate, Colloidal, Dissolved)
A comparison of background dissolved Zn concentrations measured by spICP-MS is presented for the raw, settled, and 0.02 μm filtered samples (**Table 2**). The 0.02 μm sample approximates the truly dissolved fraction of Zn, as filtration removes all but the smallest of particulates. Differences in the Zn baseline between the raw and settled samples suggest that particles with low Zn mass (**Figure 2B**) are being removed by settling (**Table 2**). The total amount of Zn present in the settleable particulate fraction (**Figure 6** and **Supplementary Table S4**) varied anywhere from 15–83% of the total Zn across the watershed. The highest absolute particulate mass concentrations were found in Sand Creek (ESC, 6.4 μg/L; WSC, 6.7 μg/L, **Supplementary Table S3**). Sand creek also had the highest turbidity values and high TR Zn, suggesting that Zn
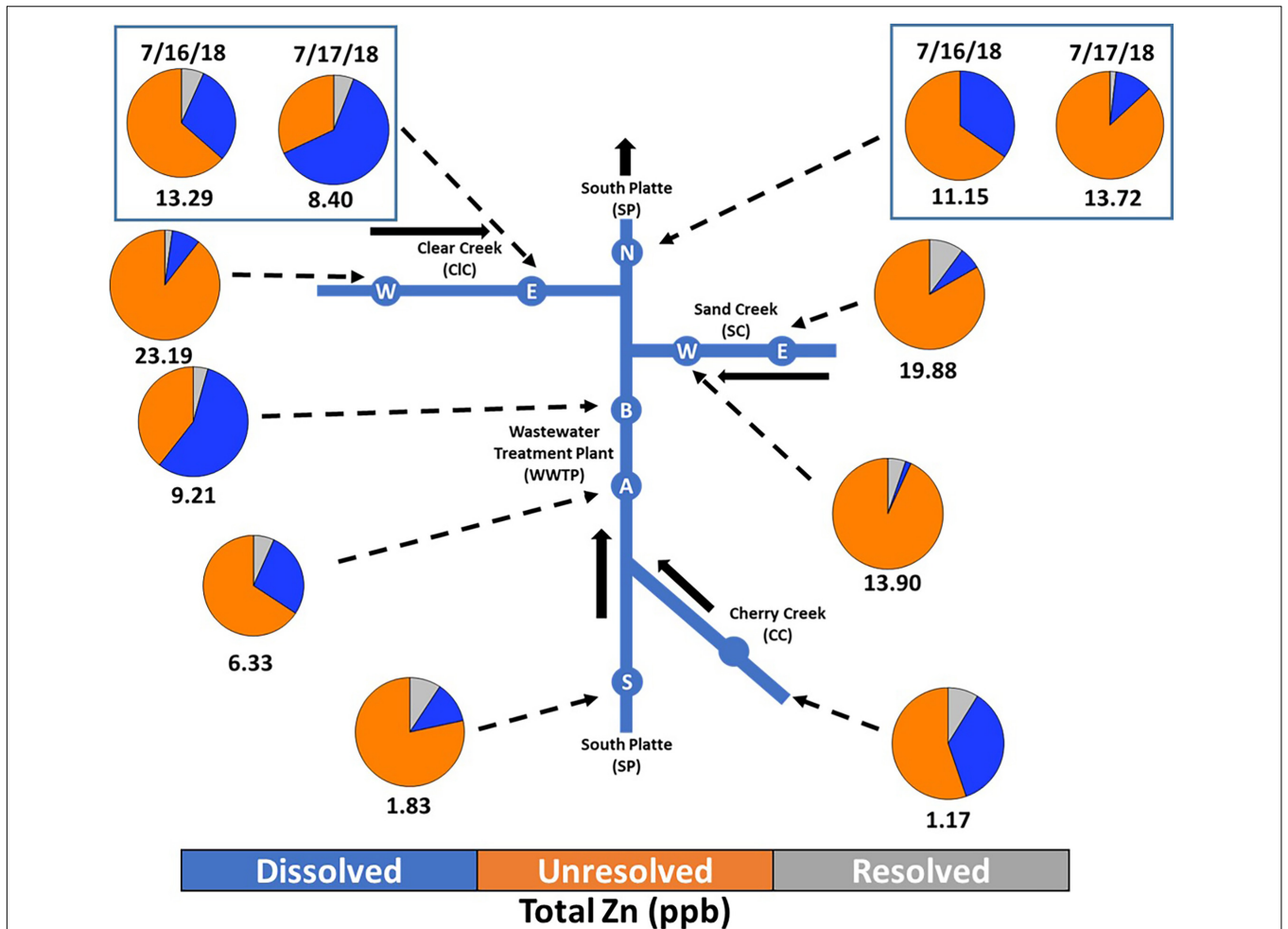
FIGURE 4 | Distribution of resolved, dissolved, and non-resolved zinc species at the various sampling locations. Bolded numbers represent total zinc concentrations in μg/L. N, S, E, and W represent the cardinal directions where "A" and "B" represent above and below the Wastewater Treatment plant, respectively.
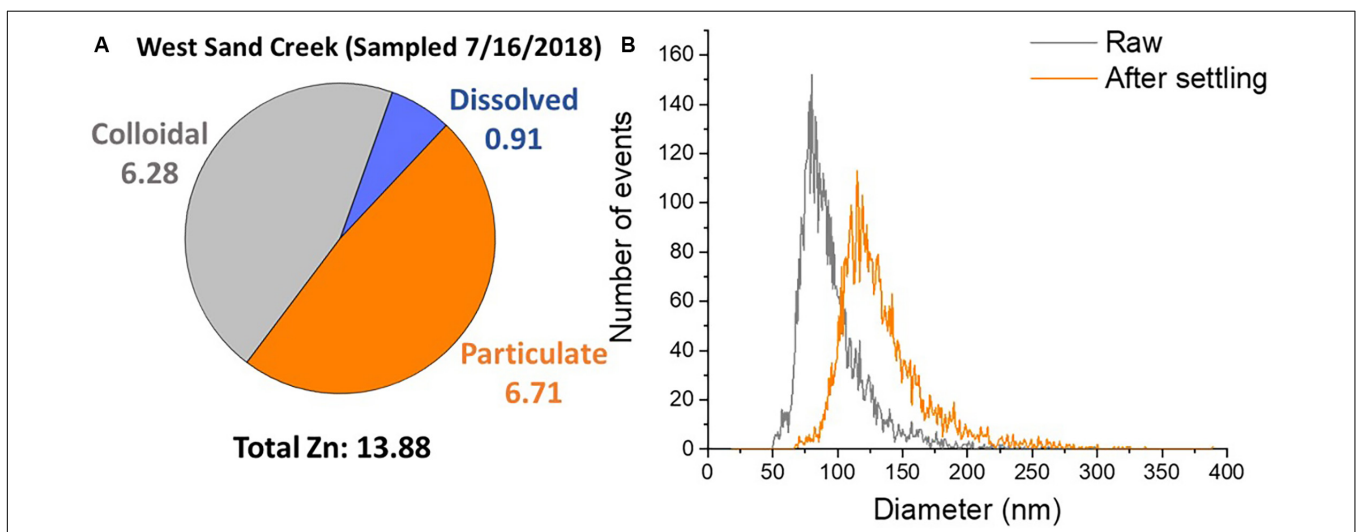

FIGURE 5 | (A) Distribution of zinc species in West sand creek (7/16/2018), concentrations in ppb, **(B)** Size distribution of raw vs. settled detected zinc events computed using ZnO density = 5.61 and a spherical geometry.

FIGURE 6 | Distribution of zinc speciation obtained by settling and 0.02 μm filtration across the watershed. N, S, E, and W represent the cardinal directions where "A" and "B" represent above and below the Wastewater Treatment plant, respectively.
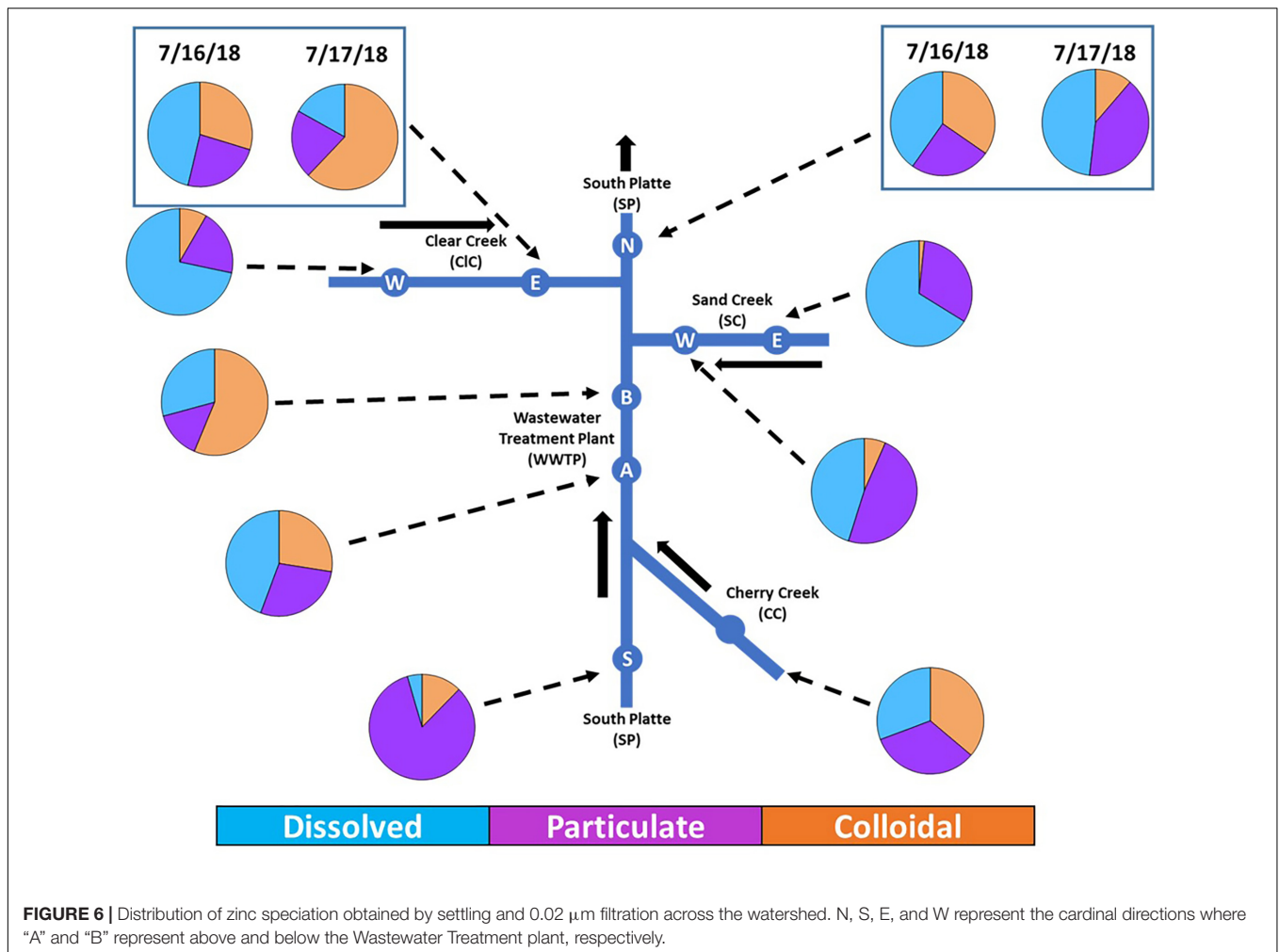
may be present adsorbed to larger sediment particles. This is corroborated by the high concentrations of settleable Zn. As noted previously the ratio of Zn to turbidity is lowest for Sand Creek, perhaps reflecting the transport of sediment from the less-urbanized eastern side of the watershed.

The colloidal portion of the total Zn (**Figure 6**) varied greatly across the watershed from 5–72% with the highest concentrations in West Clear Creek and East Sand Creek (WClC, 16.62 μg/L; ESC 13.15 μg/L). Although the particulate and colloidal fractions form a higher proportion of the total Zn contributed by southern tributaries (SSP, CC), the higher absolute values of total Zn from the western and eastern inputs (WClC, WSC/ESC) makes these the significant sources of particulate Zn.

Particle Analysis (spICP-QMS)
Integrated Zn Mass Concentration Across Watershed (Recovery Compared to TR)
The percent recovery of Zn, defined as the total concentration measured by spICP-MS divided by the TR concentration measured by ICP-OES, varied from 20–38% with a mean of 28% across the watershed (**Table 1**). The low percent recovery measured for the spICP-MS could be attributed to Zn contained

in particles larger than what can be measured by the ICP-MS. The maximum size limit for the sp-ICP-MS is based on both the need to avoid clogging of the nebulizer and the maximum-sized particle that can be completely transported through the spray chamber and ablated by the plasma. A study of silica nanoparticles in spICP-MS suggests that the maximum ablation size is upwards of 1200 nm (Olesik and Gray, 2012; Montano et al., 2016). Analysis of TR metal requires sample acidification, which liberates an indeterminate amount of the Zn contained in these larger particles, resulting in the higher TR Zn concentrations. As was previously noted, settled sediments were observed after acid digestion in some cases, especially the Sand Creek samples. Since the focus of this study is the nanoparticulate fraction, the low recovery is not of great concern but highlights that larger sediments need consideration if particulate-associated metal transport is of concern.

Resolved vs Unresolved Mass Concentration
Additional fractionation was performed to gain more insights into the speciation of colloidal/NP Zn. One such analysis was to measure the dissolved Zn concentration in 0.02 μm filtered samples. It was hypothesized that the Zn baseline "dissolved"
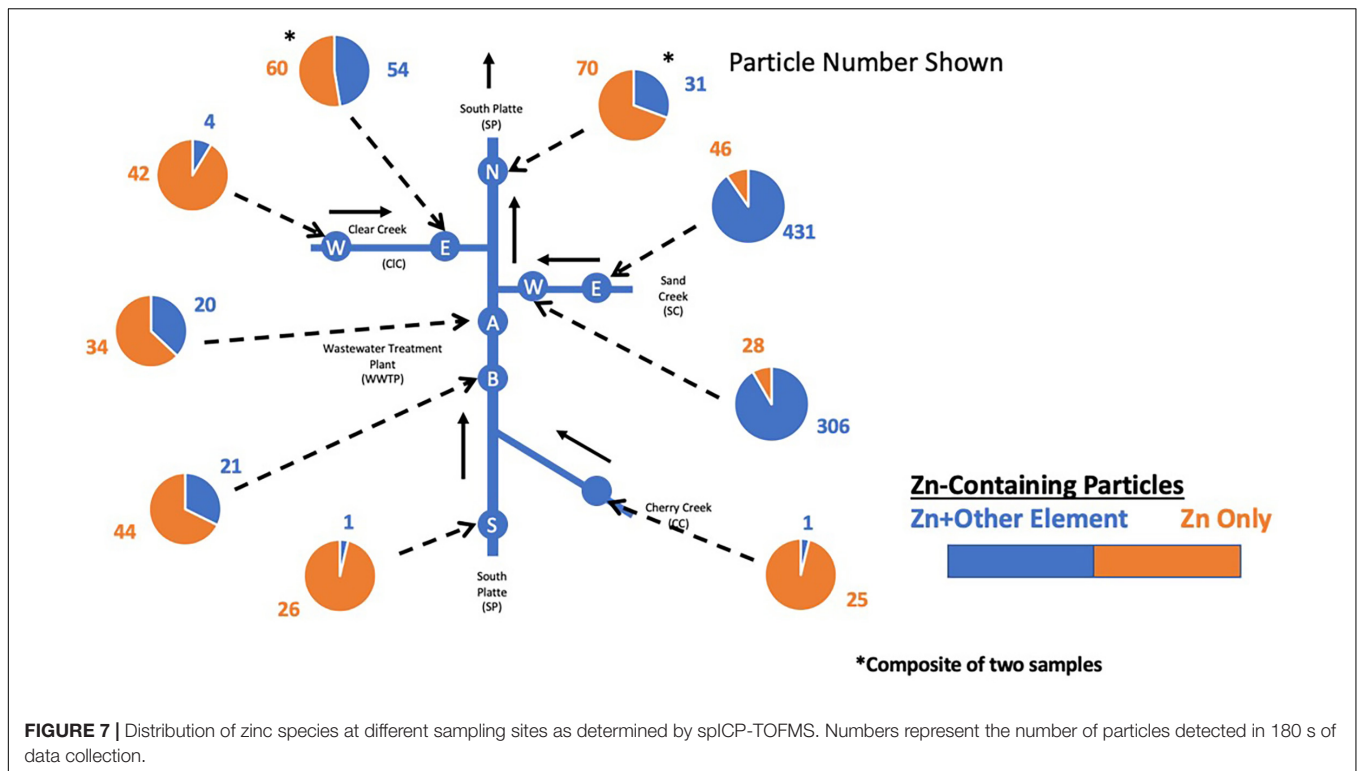
FIGURE 7 | Distribution of zinc species at different sampling sites as determined by spICP-TOFMS. Numbers represent the number of particles detected in 180 s of data collection.
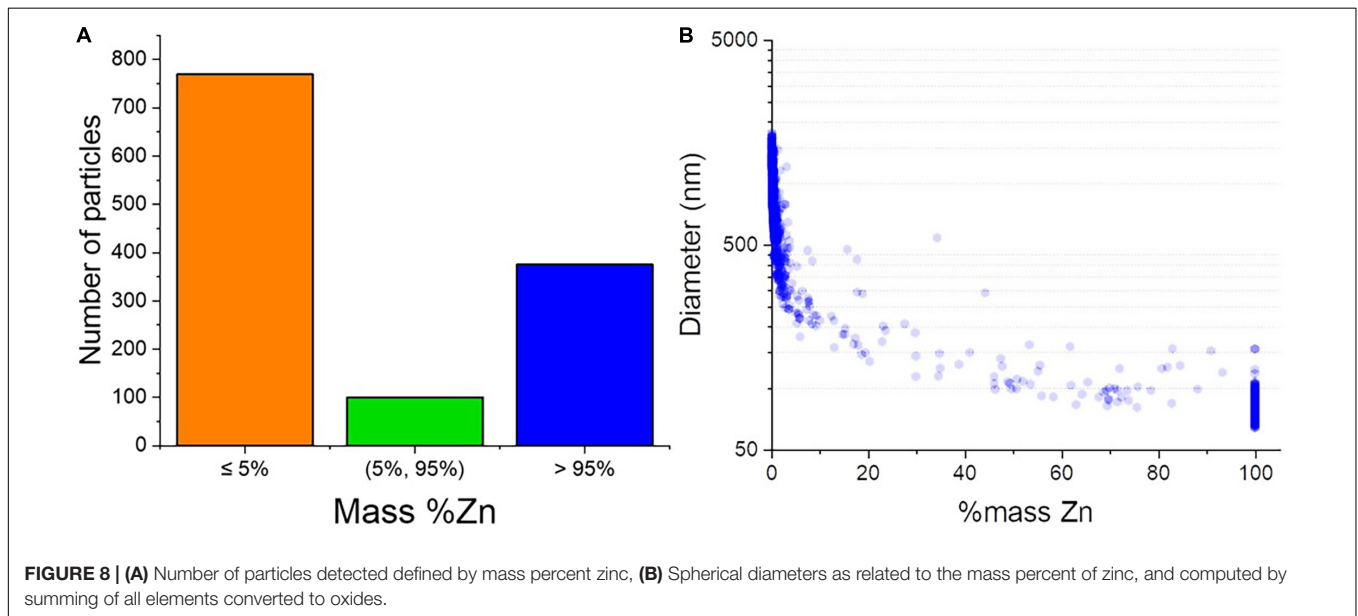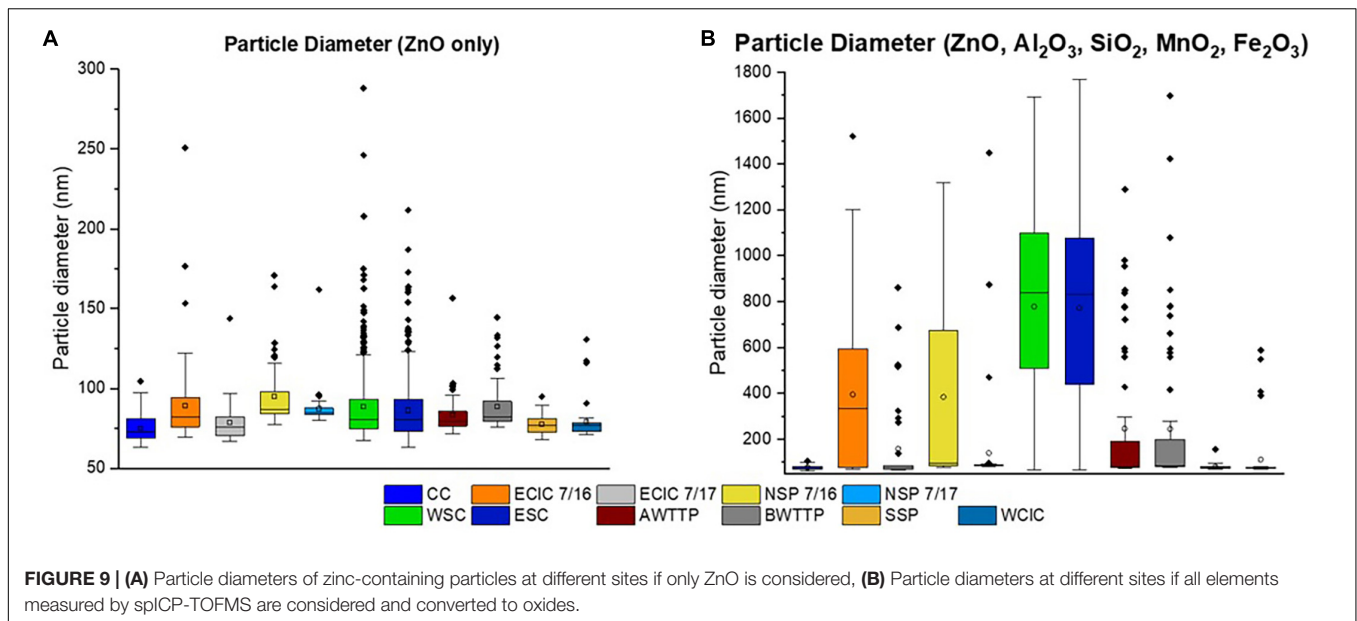

FIGURE 8 | (A) Number of particles detected defined by mass percent zinc, **(B)** Spherical diameters as related to the mass percent of zinc, and computed by summing of all elements converted to oxides.

signal, obtained for raw samples, contained a large fraction of colloidal Zn that was not massive enough to exceed the size detection limit required to be registered as a particle. Filtration was chosen over dilution for examining this size fraction, as dilution may cause dissolution and/or disaggregation of particles, resulting in artificial changes to the mass distributions (Baalousha, 2009). Although the amount of "dissolved" Zn (i.e., baseline concentration of raw samples) was greatly reduced through filtration, the 0.02 µm filtered samples still had particles

roughly 50–60 nm in mean diameter suggesting that some particles can still pass. This may also be a consequence of non-spherical shapes passing through the filter. Moreover, these particle detections may also be false positives due to their proximity to the size detection limit (45 nm) (Lee et al., 2014). Though particle information (i.e., size and number) cannot be obtained for the URNP fraction in this approach, it does provide insight into the mass concentration. Characterization of this URNP fraction of Zn is important as these small particles

FIGURE 9 | (A) Particle diameters of zinc-containing particles at different sites if only ZnO is considered, **(B)** Particle diameters at different sites if all elements measured by spICP-TOFMS are considered and converted to oxides.

may possess nano-characteristics (high specific surface area, bioavailability) different than their ionic and suspended sediment counterparts (Nel et al., 2006, 2009). Across the watershed these unresolved fractions represent greater than 50% of the Zn mass concentration (**Figure 4**), highlighting the importance of the smaller size fraction of NPs. Based on these results, more studies comparing filtration and dilution as fractionation techniques to better resolve the smallest NPs might provide a deeper understanding of nanomaterial transport and potential ecotoxicological risk.

Particle Number, Particle Mass Concentration, and Particle Mass (Size) Distributions

Across the South Platte Watershed, the number concentrations of Zn-containing particles measured by spICP-QMS were all within an order of magnitude ($\sim$60,000–220,000 particles/mL) with no higher particle numbers measured in the South Platte as compared to its tributaries (**Figure 2A**). Included in the data is a number concentration recorded for the NSP sample collected on 7/16/18 that is not in agreement with the sample collected on 7/18/18 or consistent with the value for the total Zn in the 7/16/18 sample. This result is considered an error particle counting but does not affect the integrated mass concentrations (i.e., Zn counts). The highest number concentration was observed in the Sand Creek samples, consistent with the high turbidity measured for these samples. Mean particle Zn mass (**Figure 2B**) across all sites was within an order of magnitude (1–10 fg Zn/particle). Overall, the lack of increase in the NP number concentration or variation in NP Zn mass as the South Platte flows through the urban corridor suggests either no substantial anthropogenic contribution of resolvable Zn NPs or that these measures are insensitive to urban impacts.

One notable trend is that the total Zn mass concentrations (**Figure 4**) were lower in the southern inputs to the South Platte (CC and SSP) compared to the urban sites downstream (AWWTP, BWTTP, and NSP). The higher Zn mass concentrations in all three fractions (dissolved, unresolved, and resolved particles) in the downstream sites suggest that the urban environment is contributing Zn to the watershed. Both SSP and CC have a significant water impoundment upstream of them, Chatfield and Cherry Creek Reservoirs, respectively. These reservoirs likely act as a settling basin for particulate and sediment, reducing the background of NNP and increasing the magnitude of the urban effect. Chatfield Reservoir sits on the southwestern edge of the urbanized Denver metro area and thus could be expected to act as a settling basin for NNP but have little effect on anthropogenic or natural particles added to the watershed by the city itself. Among potential INPs, tire wear particles (Dahl et al., 2006; Klöckner et al., 2019) and brake dust (Adachi and Tainosho, 2004) are two likely sources of Zn particles in an urban watershed; as their presence in areas adjacent to roadways has been well-documented in soil, air and stormwater (Baalousha et al., 2016). The Sand Creek site produced two samples with high Zn mass concentrations, which were principally contained in the resolved and unresolved particle fractions. Examination of the hydrographs around the watershed (**Supplementary Figure S1**) shows that the rain event on July 15th. 2018 had considerable impact on Sand Creek. Flow increased by seven-fold from the event and this was the largest increase in flow of any South Platte tributary proportional to base flow. The increase in Zn particles, both resolved and non-resolved (**Figure 4**), could possibly thus be attributed to the rainfall pattern and the high volume of rainwater washing particles into Sand Creek and resuspending bed sediment. West Clear Creek is another tributary where high amounts of resolved and non-resolved Zn particles were observed (**Figure 4**) and these particles may be the result of widespread abandoned metal sulfide mines in the upper Clear Creek watershed (Butler, 2009).

Although the study focuses on the variation in concentration (mass and number) and chemical characteristics of Zn-containing particles within the urban watershed, it is useful to examine other information obtained by spICP-QMS, namely the particle mass (i.e., size) distributions (SI **Figure 3**). The lack of particles detected at small sizes (**Figure 5B**, computed for this example using a density of ZnO, 5.61 g/cm^3), despite the limit of detection being an ample distance below the mean measured size, resulted in size distributions that appear approximately gaussian. With high dissolved Zn backgrounds, smaller particles that register close to the average background can be obscured. However, in these data sets the dissolved background does not fully account for the absence of smaller NPs. For example, based on the instrumental noise and the dissolved background, for East Sand Creek, the limit of detection is estimated to be 55 nm, well below the leading edge of the particle distribution at roughly 77 nm (**Figure 5B**). Whether the measured particle size distributions are abnormal for this type of analysis is an open question. Pareto's law suggests that particle distributions in the environment should follow a power law relationship between size and number, namely as particles get smaller, their number should exponentially increase (Walther et al., 2006). Numerous studies have found that observed particle distributions can follow this law, (Baur et al., 2020) display a Poisson distribution (Dahl et al., 2006; Hadioui et al., 2015), or even be bimodal (Lin et al., 2005). These studies highlight many possible causes to explain distributions not following Pareto's law include influence of the type of sample (sediment vs. aqueous) or particle source (road wear vs. atmospheric). Thus, the lack of an observed monotonically decreasing number-based size distribution may arise from real effects or from analytical artifacts. ENP may not behave according to Pareto's law in that they are manufactured and perhaps introduced into the environment with a more defined size distribution. Natural processes such as weathering, that produce NP, could adhere to the law more closely as nanoparticles are not the starting material but a product of a bulk transformation. Another analytical explanation for the observed particle size distributions is that although NPs may be present in the "gap" between the DL and the maximum of the distribution, random variation in NP-generated signal results in their partial undercounting when close to the background noise level (i.e., some particle generate counts below the 3σ size DL). Regardless of cause, for very polydisperse natural samples, the counting statistics obtained in this study may not be sufficient to draw a conclusion regarding the distribution shape. Previous studies (Laborda et al., 2013) have suggested that 10^5 particles counted are necessary for a firm conclusion about particle size and have found a 3–10% variation in measured sizes. These are valid concerns that must be addressed in future field-based studies of NP size distributions.

Settling Particle Results (Number, Size, Background/Dissolved)

In addition to filtration, settling experiments were a means of discerning more about the speciation of Zn particles present in the resolved (RP) and unresolved URNP fractions. **Figure 5A**

compares the distribution of particle masses for the settled and raw samples of West Sand Creek (7/16/18). Both raw and settled samples had approximately the same number of particles (Raw, 4482 particles; Settled, 4820 particles) but their mean diameter was different (Raw, 134 nm; Settled, 103 nm). In the time-frame used, the 100–200 nm particle distribution (**Figure 5B**) should not have been affected if particles were zinc metal or ZnO. Background Zn concentrations for the raw and settled samples were 13.90 and 7.19 ppb, respectively, with a dissolved Zn concentration for the site (0.02 μm filtered sample) was 0.91 ppb. It is apparent from the decrease in mean particle diameter and background Zn concentration in the settled sample, that settling removed Zn from solution even though the resolved Zn particles in the raw sample had a size distribution well below the calculated settleable size. A likely explanation is that part of the Zn measured in the raw sample is associated (either adsorbed or as a minor component) of larger minerals and hetero-aggregates. These larger particles containing low amounts of Zn could avoid detection as a resolvable Zn particle by the spICP-QMS. Thus, their absence from solution would be noted by a decrease in the background Zn concentration. This approach allows one to use spICP-QMS to gather more indirect evidence on the nature of metal-containing NPs but also leads direct to the obvious need for multi-element NP analysis.

Particle Analysis (spICP-TOFMS)

Given the varying morphologies and speciation of Zn, spICP-TOFMS was employed to quantify multiple elements within each particle (**Figure 7**). One inherent advantage of the ICP-TOFMS is the ability to distinguish between particles composed only of Zn (as the cation) and those that contain additional elements (excluding O, S, and other non-ionizable elements). This distinction is important in attempting to separate particles of anthropogenic origin from those of natural origin. Anthropogenic particles (i.e., tire wear, ENPs) are more likely to contain Zn as the only or primary metallic element. NNP with adsorbed Zn would contain other elements at amounts above that of Zn. Similarly, mineral NPs containing Zn within their lattice and hetero-aggregates of Zn-NPs and NNPs would also have some proportion of Zn but are likely to be principally composed of other elements.

It is important to note that fewer particles were counted by spICP-TOFMS, amounting to 10–20% that of the quadrupole instrument (**Figure 7**). Due to the difference in dwell times between the quadrupole and TOF instruments, 0.1 and 3 ms, respectively, considerable dilution for the TOF experiments was necessary to avoid coincidence of particles within one dwell time. The 1:1000 dilution used in these experiments for the TOF measurements is the most likely cause of the low particle numbers detected by the TOF, however, instrument sensitivity differences are also a possible cause. Data acquisition over a longer time period could be used to offset dilution differences and thus generate a comparable number of particles for both techniques.

Across all sites, similar average masses of Zn per particle were found in the Zn-only particles. Converting these masses to diameters, and assuming all the Zn is present as spherical ZnO NPs (**Figure 9A**), these particles were roughly 80 nm

in diameter, most values falling within 20 nm of this average value. We obtained a similar result for all Zn-containing NP when using an ICP-QMS, which provides only a single element analysis, concluding that the measured Zn NPs are relatively similar in size and composition across the South Platte watershed. However, with a TOF detector we can consider the other elements present in each particle, in this case Fe, Mn, Al, and Si, which imply a more complex mineralogy for the Zn-containing particles. Mineral particles can promote adsorption, particularly the common metal oxides (Fe, Mn; Trivedi and Axe, 2000), and aluminosilicate clays (Al, Si) (Sheikhhosseini et al., 2013). Converting the mass of each element to an oxide (Fe_2O_3, MnO_2, SiO_2, and Al_2O_3), assuming a density and spherical geometry, and combining them with mass of ZnO from the previous figure, we can approximate a more likely size of the particles (**Figure 9B**). It should be noted that some of these sizes are approaching the theoretical upper limit for spICP-MS, and thus might be underrepresenting the largest of the particle sizes. Plotting all particles by total oxide equivalent spherical size vs %m Zn (**Figure 8B**), we find a clear relationship with low % zinc being uniformly large (200–1000 nm) and high % zinc being uniformly small (60–100 nm).

The disconnect between the ZnO-only particle size and the particle size where all five elements are considered allows us to tease out differences in Zn particle speciation. Zn-containing particles where the Zn is adsorbed or hetero-agglomerated should show a large deviation between the particle radii calculated when considering ZnO only vs all five elements. It is expected that the Zn-adsorbed/aggregated particles would primarily be composed of other elements besides Zn and thus have only a small proportion of the total mass as Zn. This bears out for the size distributions of sampling sites such as Sand Creek, East Clear Creek and North South Platte (7/16/18), where the ZnO-only radius is much smaller than the radius of particles where all elements were considered (**Figures 9A,B**). For Sand Creek, the higher proportion of Zn possibly contained as an adsorbate also supports the settling experiments utilizing the ICP-QMS. A high proportion of the Zn particles present in the Sand Creek samples could thus be classified as sediment particles with adsorbed Zn. Conversely, the small difference between Zn-only and multi-element particle size (**Figures 9A,B**) suggest that NPs primarily composed of Zn dominated other locations along the South Platte such as the wastewater treatment plant sites (AWTTP, BWTTP). This may be some indication of a greater anthropogenic contribution.

Separating particles based on the percentage of their % Zn mass also allowed for better speciation of the particle-associated Zn in a sample. The different chemical properties of nanoparticulate Zn as compared to dissolved metal ions or adsorbed Zn is well known. ZnO and other metal oxide nanoparticles are potent reactive oxygen species generators and have ecotoxicity characteristics distinct from the dissolved forms of the metals (Xia et al., 2008). Adsorption of heavy metals to nanoparticles is an important component of many biogeochemical cycles and identifying the prevalence of adsorbed metal can be a boon to modeling and environmental remediation (Hochella et al., 2005).

Dissolution studies have shown ZnO can be soluble (7–16 mg/mL; Franklin et al., 2007; Reed et al., 2012a; Domingos et al., 2013; Ma et al., 2013) at the pH values expected for these surface waters (pH 7-8). However, ZnO dissolution can be affected by inorganic factors including water hardness (Reed et al., 2012b), and pH (Miao et al., 2010; Domingos et al., 2013) or organic species such as fulvic acids, NOM (Domingos et al., 2013) or protein (Moreau et al., 2007). Also, ZnO may compose up to 1% by weight of the total tire mass (Milani et al., 2004) and ZnO particles from tire wear may be embedded in rubber, protecting them from solubilization. ZnO may also be protected from dissolution by being coated by a less soluble Zn mineral such as $ZnCO_3$ (Reed et al., 2012b). Based on the host of factors that can affect ZnO particle dissolution, it seems highly possible that ZnO NP could be present in natural waters.

Future studies might be improved by including transmission electron microscopy (TEM) or scanning electron microscopy (SEM) to identify the chemical speciation of Zn particles be they ZnO, ZnS, $ZnCO_3$, or a more exotic metal compound. However, the ppb levels, which results in low particle numbers, make observing these particles by EM very difficult. Other particle characterization techniques, such as FFF, might also provide valuable information by providing an additional means by which to verify the size of the particles whilst characterizing their elemental composition. Employing fraction collection of the FFF eluent would also permit additional characterization by spICP-MS (Kly et al., 2020). The identification of the exact Zn particle mineralogy could also aid in determination of their origin and determining a truer particle size. Similarly, Fe, Mn, Al, and Si were assumed to be oxides for the purposes of calculating a particle size. This assumption was made for simplicity sake but does not reflect the probability that these elements are most likely present as a variety of aluminosilicate minerals. More detailed analysis of the mineralogy present in these samples would allow for more accurate representations of particle size where these elements are considered, although determining the association of Zn with the observed minerals is problematic at the low (<5%) Zn contents observed in these waters.

CONCLUSION

By utilizing sp-ICP-MS, using both a quadrupole and a time-of-flight detector, the NP populations present in an urban watershed could be more fully characterized. The unique use of settling and filtration experiments combined with an ICP-QMS provided further speciation of metal-containing particles using single element data. ICP-TOFMS analysis provided invaluable insights into the elemental abundances (i.e., mineralogy) present on a particle-by-particle basis. The totality of these analyses allows for the further speciation of metal-containing particles into particles composed completely of a given metal, and those with the metal adsorbed to, or incorporated within, colloidal mineral matter. This survey of the South Platte watershed found that Zn-only particles were more abundant in the central, more urbanized parts of the watershed, suggesting, but not confirming, anthropogenic origin. ZnO nanoparticles from tire wear particles

were hypothesized, but not investigated, as the most likely source. If regulation is in the future for nanomaterial emissions, the ability to distinguish between particle types will be invaluable. Most significantly, the study demonstrates that multi-elemental information, provided by an ICP-TOFMS, may form the future basis for developing the field of particle-by-particle geology, utilizing each particles elemental composition. Furthermore, a variety of different information about metal speciation can be derived from the application of settling and filtration as fractionation tools prior to ICP-QMS analysis.

DATA AVAILABILITY STATEMENT

The raw data supporting the conclusions of this article will be made available upon request by the authors, without undue reservation, to any qualified researcher.

AUTHOR CONTRIBUTIONS

SB, MM, and JR equally contributed to the writing of this manuscript. SB and LR performed sampling, filtration and settling experiments, and ICP-QMS measurements under the direction of JR. MM performed the spICP-TOFMS experiments and measurements under the guidance of TH and FK. All authors contributed to the article and approved the submitted version.

SUPPLEMENTARY MATERIAL

The Supplementary Material for this article can be found online at: https://www.frontiersin.org/articles/10.3389/fenvs.2020.00084/full#supplementary-material

REFERENCES

Adachi, K., and Tainosho, Y. (2004). Characterization of heavy metal particles embedded in tire dust. *Environ. Int.* 30, 1009–1017. doi: 10.1016/j.envint.2004.04.004

Baalousha, M. (2009). Aggregation and disaggregation of iron oxide nanoparticles: influence of particle concentration, pH and natural organic matter. *Sci. Total Environ.* 407, 2093–2101. doi: 10.1016/j.scitotenv.2008.11.022

Baalousha, M., Yang, Y., Vance, M. E., Colman, B. P., McNeal, S., Xu, J., et al. (2016). Outdoor urban nanomaterials: the emergence of a new, integrated, and critical field of study. *Sci. Total Environ.* 557, 740–753. doi: 10.1016/j.scitotenv.2016.03.132

Baur, S., Reemtsma, T., Stärk, H.-J., and Wagner, S. (2020). Surfactant assisted extraction of incidental nanoparticles from road runoff sediment and their characterization by single particle-ICP-MS. *Chemosphere* 246, 125765. doi: 10.1016/j.chemosphere.2019.125765

Borovinskaya, O., Hattendorf, B., Tanner, M., Gschwind, S., and Gunther, D. (2013). A prototype of a new inductively coupled plasma time-of-flight mass spectrometer providing temporally resolved, multi-element detection of short signals generated by single particles and droplets. *J. Anal. Atomic Spectrom.* 28, 226–233. doi: 10.1039/c2ja30227f

Butler, B. A. (2009). Effect of pH, ionic strength, dissolved organic carbon, time, and particle size on metals release from mine drainage impacted streambed sediments. *Water Res.* 43, 1392–1402. doi: 10.1016/j.watres.2008.12.009

Councell, T. B., Duckenfield, K. U., Landa, E. R., and Callender, E. (2004). Tire-wear particles as a source of zinc to the environment. *Environ. Sci. Technol.* 38, 4206–4214. doi: 10.1021/es034631f

Dahl, A., Gharibi, A., Swietlicki, E., Gudmundsson, A., Bohgard, M., Ljungman, A., et al. (2006). Traffic-generated emissions of ultrafine particles from pavement–tire interface. *Atmosp. Environ.* 40, 1314–1323. doi: 10.1016/j.atmosenv.2005.10.029

DeForest, D. K., and Van Genderen, E. J. (2012). Application of US EPA guidelines in a bioavailability-based assessment of ambient water quality criteria for zinc in freshwater. *Environ. Toxicol. Chem.* 31, 1264–1272. doi: 10.1002/etc.1810

Domingos, R. F., Rafiei, Z., Monteiro, C. E., Khan, M. A., and Wilkinson, K. J. (2013). Agglomeration and dissolution of zinc oxide nanoparticles: role of pH, ionic strength and fulvic acid. *Environ. Chem.* 10, 306–312.

Erhardt, T., Jensen, C. M., Borovinskaya, O., and Fischer, H. (2019). Single particle characterization and total elemental concentration measurements in polar ice using continuous flow analysis-inductively coupled plasma time-of-flight mass spectrometry. *Environ. Sci. Technol.* 53, 13275–13283. doi: 10.1021/acs.est.9b03886

Ermolin, M., Fedotov, P., Ivaneev, A., Karandashev, V., Fedyunina, N., and Eskina, V. (2017). Isolation and quantitative analysis of road dust nanoparticles. *J. Anal. Chem.* 72, 520–532. doi: 10.1134/s1061934817050057

Franklin, N. M., Rogers, N. J., Apte, S. C., Batley, G. E., Gadd, G. E., and Casey, P. S. (2007). Comparative toxicity of nanoparticulate ZnO, bulk ZnO, and ZnCl2 to a freshwater microalga (Pseudokirchneriella subcapitata): the importance of particle solubility. *Environ. Sci. Technol.* 41, 8484–8490. doi: 10.1021/es071445r

Fréchette-Viens, L., Hadioui, M., and Wilkinson, K. J. (2019). Quantification of ZnO nanoparticles and other Zn containing colloids in natural waters using a high sensitivity single particle ICP-MS. *Talanta* 200, 156–162. doi: 10.1016/j.talanta.2019.03.041

Furtado, L. M., Hoque, M. E., Mitrano, D. F., Ranville, J. F., Cheever, B., Frost, P. C., et al. (2014). The persistence and transformation of silver nanoparticles in littoral lake mesocosms monitored using various analytical techniques. *Environ. Chem.* 11, 419–430. doi: 10.1071/En14064

Giese, B., Klaessig, F., Park, B., Kaegi, R., Steinfeldt, M., Wigger, H., et al. (2018). Risks, release and concentrations of engineered nanomaterial in the environment. *Sci. Rep.* 8, 1–18.

Gondikas, A., von der Kammer, F., Kaegi, R., Borovinskaya, O., Neubauer, E., Navratilova, J., et al. (2018). Where is the nano? Analytical approaches for the detection and quantification of TiO 2 engineered nanoparticles in surface waters. *Environ. Sci. Nano* 5, 313–326. doi: 10.1039/c7en00952f

Gondikas, A. P., von der Kammer, F., Reed, R. B., Wagner, S., Ranville, J. F., and Hofmann, T. (2014). Release of TiO2 nanoparticles from sunscreens into surface waters: a one-year survey at the old danube Recreational Lake. *Environ. Sci. Technol.* 48, 5415–5422. doi: 10.1021/es405596y

Gonet, T., and Maher, B. A. (2019). Airborne, vehicle-derived fe-bearing nanoparticles in the urban environment: a review. *Environ. Sci. Technol.* 53, 9970–9991. doi: 10.1021/acs.est.9b01505

Gschwind, S., Flamigni, L., Koch, J., Borovinskaya, O., Groh, S., Niemax, K., et al. (2011). Capabilities of inductively coupled plasma mass spectrometry for the detection of nanoparticles carried by monodisperse microdroplets. *J. Anal. Atomic Spectrom.* 26, 1166–1174. doi: 10.1039/c0ja00249f

Hadioui, M., Merdzan, V., and Wilkinson, K. J. (2015). Detection and characterization of ZnO nanoparticles in surface and waste waters using single particle ICPMS. *Environ. Sci. Technol.* 49, 6141–6148. doi: 10.1021/acs.est.5b00681

Hegetschweiler, A., Borovinskaya, O., Staudt, T., and Kraus, T. (2018). Single-particle mass spectrometry of titanium and niobium carbonitride precipitates in steels. *Anal. Chem.* 91, 943–950. doi: 10.1021/acs.analchem.8b04012

Hendren, C. O., Mesnard, X., Droge, J., and Wiesner, M. R. (2011). Estimating production data for five engineered nanomaterials as a basis for exposure assessment. *Environ. Sci. Technol.* 45, 2562–2569. doi: 10.1021/es103300g

Hendriks, L., Gundlach-Graham, A., Hattendorf, B., and Guther, D. (2017). Characterization of a new ICP-TOFMS instrument with continuous and discrete introduction of solutions. *J. Anal. Atom. Spectrom.* 32, 548–561. doi: 10.1039/c6ja00400h

Heringer, R. D., and Ranville, J. F. (2018). Gunshot residue (GSR) analysis by single particle inductively coupled plasma mass spectrometry (spICP-MS). *For. Sci. Int.* 288, e20–e25. doi: 10.1016/j.forsciint.2018.05.010

Herzog, B., Mongiat, S., Deshayes, C., Neuhaus, M., Sommer, K., and Mantler, A. (2002). In vivo and in vitro assessment of UVA protection by sunscreen formulations containing either butyl methoxy dibenzoyl methane, methylene bis-benzotriazolyl tetramethylbutylphenol, or microfine ZnO. *Int. J. Cosmetic Sci.* 24, 170–185. doi: 10.1046/j.1467-2494.2002.00137.x

Hochella, M. F. Jr., Lower, S. K., Maurice, P. A., Penn, R. L., Sahai, N., Sparks, D. L., et al. (2008). Nanominerals, mineral nanoparticles, and Earth systems. *Science* 319, 1631–1635. doi: 10.1126/science.1141134

Hochella, M. F. Jr., Moore, J. N., Putnis, C. V., Putnis, A., Kasama, T., and Eberl, D. D. (2005). Direct observation of heavy metal-mineral association from the clark fork river superfund complex: implications for metal transport and bioavailability. *Geochim. Cosmochim. Acta* 69, 1651–1663. doi: 10.1016/j.gca.2004.07.038

Hochella, M. F., Mogk, D. W., Ranville, J., Allen, I. C., Luther, G. W., Marr, L. C., et al. (2019). Natural, incidental, and engineered nanomaterials and their impacts on the Earth system. *Science* 363:eaau8299. doi: 10.1126/science.aau8299

Kaiser, J.-P., Zuin, S., and Wick, P. (2013). Is nanotechnology revolutionizing the paint and lacquer industry? A critical opinion. *Sci. Total Environ.* 442, 282–289. doi: 10.1016/j.scitotenv.2012.10.009

Klöckner, P., Reemtsma, T., Eisentraut, P., Braun, U., Ruhl, A. S., and Wagner, S. (2019). Tire and road wear particles in road environment–Quantification and assessment of particle dynamics by Zn determination after density separation. *Chemosphere* 222, 714–721. doi: 10.1016/j.chemosphere.2019.01.176

Kly, S., Moffitt, M., Rand, L., and Ranville, J. F. (2020). Coupling single particle ICP-MS with field-flow fractionation for characterizing metal nanoparticles contained in nanoplastic colloids. *Environ. Sci.* 43, 7277–7284.

Laborda, F., Bolea, E., and Jimenez-Lamana, J. (2014). Single particle inductively coupled plasma mass spectrometry: a powerful tool for nanoanalysis. *Anal. Chem.* 86, 2270–2278. doi: 10.1021/ac402980q

Laborda, F., Jimenez-Lamana, J., Bolea, E., and Castillo, J. R. (2013). Critical considerations for the determination of nanoparticle number concentrations, size and number size distributions by single particle ICP-MS. *J. Anal. Atomic Spectrom.* 28, 1220–1232. doi: 10.1039/c3ja50100k

Lamprea, K., Bressy, A., Mirande-Bret, C., Caupos, E., and Gromaire, M.-C. (2018). Alkylphenol and bisphenol A contamination of urban runoff: an evaluation of the emission potentials of various construction materials and automotive supplies. *Environ. Sci. Pollut. Res.* 25, 21887–21900. doi: 10.1007/s11356-018-2272-z

Lee, S., Bi, X., Reed, R. B., Ranville, J. F., Herckes, P., and Westerhoff, P. (2014). Nanoparticle size detection limits by single particle ICP-MS for 40 elements. *Environ. Sci. Technol.* 48, 10291–10300. doi: 10.1021/es502422v

Lin, C.-C., Chen, S.-J., Huang, K.-L., Hwang, W.-I., Chang-Chien, G.-P., and Lin, W.-Y. (2005). Characteristics of metals in nano/ultrafine/fine/coarse particles collected beside a heavily trafficked road. *Environ. Sci. Technol.* 39, 8113–8122. doi: 10.1021/es048182a

Ma, R., Levard, C., Michel, F. M., Brown, G. E. Jr., and Lowry, G. V. (2013). Sulfidation mechanism for zinc oxide nanoparticles and the effect of sulfidation on their solubility. *Environ. Sci. Technol.* 47, 2527–2534. doi: 10.1021/es3035347

Miao, A. J., Zhang, X. Y., Luo, Z., Chen, C. S., Chin, W. C., Santschi, P. H., et al. (2010). Zinc oxide–engineered nanoparticles: dissolution and toxicity to marine phytoplankton. *Environ. Toxicol. Chem.* 29, 2814–2822. doi: 10.1002/etc.340

Milani, M., Pucillo, F., Ballerini, M., Camatini, M., Gualtieri, M., and Martino, S. (2004). First evidence of tyre debris characterization at the nanoscale by focused ion beam. *Mater. Characteriz.* 52, 283–288.

Montaño, M. D., Badiei, H. R., Bazargan, S., and Ranville, J. (2014). Improvements in the detection and characterization of engineered nanoparticles using spICP-MS with microsecond dwell times. *Environ. Sci.* 1, 338–346. doi: 10.1039/c4en00058g

Montano, M. D., Olesik, J. W., Barber, A. G., Challis, K., and Ranville, J. F. (2016). Single Particle ICP-MS: advances toward routine analysis of nanomaterials. *Anal. Bioanal. Chem.* 408, 5053–5074. doi: 10.1007/s00216-016-9676-8

Montaño, M. D., von der Kammer, F., Cuss, C. W., and Ranville, J. F. (2019). Opportunities for examining the natural nanogeochemical environment using recent advances in nanoparticle analysis. *J. Anal. Atom. Spectrom.* 34, 1768–177. doi: 10.1039/c9ja00168a

Moreau, J. W., Weber, P. K., Martin, M. C., Gilbert, B., Hutcheon, I. D., and Banfield, J. F. (2007). Extracellular proteins limit the dispersal of biogenic nanoparticles. *Science* 316, 1600–1603. doi: 10.1126/science.1141064

Naasz, S., Weigel, S., Borovinskaya, O., Serva, A., Cascio, C., Undas, A. K., et al. (2018). Multi-element analysis of single nanoparticles by ICP-MS using quadrupole and time-of-flight technologies. *J. Anal. Atom. Spectrom.* 33, 835–845. doi: 10.1039/c7ja00399d

Nel, A., Xia, T., Madler, L., and Li, N. (2006). Toxic potential of materials at the nanolevel. *Science* 311, 622–627. doi: 10.1126/science.1114397

Nel, A. E., Madler, L., Velegol, D., Xia, T., Hoek, E. M., Somasundaran, P., et al. (2009). Understanding biophysicochemical interactions at the nano-bio interface. *Nat. Mater.* 8, 543–557. doi: 10.1038/nmat2442

Olesik, J. W., and Gray, P. J. (2012). Considerations for measurement of individual nanoparticles or microparticles by ICP-MS: determination of the number of particles and the analyte mass in each particle. *J. Anal. Atom. Spectrom.* 27, 1143–1155. doi: 10.1039/c2ja30073g

Osmond, M. J., and McCall, M. J. (2010). Zinc oxide nanoparticles in modern sunscreens: an analysis of potential exposure and hazard. *Nanotoxicology* 4, 15–41. doi: 10.3109/17435390903502028

Pace, H. E., Rogers, N. J., Jarolimek, C., Coleman, V. A., Higgins, C. P., and Ranville, J. F. (2011). Determining transport efficiency for the purpose of counting and sizing nanoparticles via single particle inductively coupled plasma mass spectrometry. *Anal. Chem.* 83, 9361–9369. doi: 10.1021/ac201952t

Piccinno, F., Gottschalk, F., Seeger, S., and Nowack, B. (2012). Industrial production quantities and uses of ten engineered nanomaterials in Europe and the world. *J.Nanopart. Res.* 14, 1–11. doi: 10.1007/s11051-012-1109-9

Plathe, K. L., von der Kammer, F., Hassellov, M., Moore, J., Murayama, M., Hofmann, T., et al. (2010). Using FlFFF and aTEM to determine trace metal-nanoparticle associations in riverbed sediment. *Environ. Chem.* 7, 82–93. doi: 10.1071/En09111

Praetorius, A., Gundlach-Graham, A., Goldberg, E., Fabienke, W., Navratilova, J., Gondikas, A., et al. (2017). Single-particle multi-element fingerprinting (spMEF) using inductively-coupled plasma time-of-flight mass spectrometry (ICP-TOFMS) to identify engineered nanoparticles against the elevated natural background in soils. *Environ. Sci. Nano* 4, 307–314. doi: 10.1039/c6en00455e

Reed, R. B., Higgins, C. P., Westerhoff, P., Tadjiki, S., and Ranville, J. F. (2012a). Overcoming challenges in analysis of polydisperse metal-containing nanoparticles by single particle inductively coupled plasma mass spectrometry. *J. Anal. Atom. Spectrom.* 27, 1093–1100. doi: 10.1039/c2ja30061c

Reed, R. B., Ladner, D. A., Higgins, C. P., Westerhoff, P., and Ranville, J. F. (2012b). Solubility of nano-zinc oxide in environmentally and biologically important matrices. *Environ. Toxicol. Chem.* 31, 93–99. doi: 10.1002/etc.708

Reed, R. B., Martin, D. P., Bednar, A. J., Montano, M. D., Westerhoff, P., and Ranville, J. F. (2017). Multi-day diurnal measurements of Ti-containing nanoparticle and organic sunscreen chemical release during recreational use of a natural surface water. *Environ. Sci. Nano* 4, 69–77. doi: 10.1039/c6en00283h

Sheikhhosseini, A., Shirvani, M., and Shariatmadari, H. (2013). Competitive sorption of nickel, cadmium, zinc and copper on palygorskite and sepiolite silicate clay minerals. *Geoderma* 192, 249–253. doi: 10.1016/j.geoderma.2012.07.013

Shuster, W. D., Bonta, J., Thurston, H., Warnemuende, E., and Smith, D. (2005). Impacts of impervious surface on watershed hydrology: a review. *Urban Water J.* 2, 263–275. doi: 10.1080/15730620500386529

Sommer, F., Dietze, V., Baum, A., Sauer, J., Gilge, S., Maschowski, C., et al. (2018). Tire abrasion as a major source of microplastics in the environment. *Aerosol Air Qual. Res.* 18, 2014–2028. doi: 10.4209/aaqr.2018.03.0099

Stolpe, B., Hassellov, M., Andersson, K., and Turner, D. R. (2005). High resolution ICPMS as an on-line detector for flow field-flow fractionation; multi-element determination of colloidal size distributions in a natural water sample. *Anal. Chim. Acta* 535, 109–121. doi: 10.1016/j.aca.2004.11.067

Sun, T. Y., Mitrano, D. M., Bornhöft, N. A., Scheringer, M., Hungerbühler, K., and Nowack, B. (2017). Envisioning nano release dynamics in a changing world: using dynamic probabilistic modeling to assess future environmental emissions of engineered nanomaterials. *Environ. Sci. Technol.* 51, 2854–2863. doi: 10.1021/acs.est.6b05702

Toor, G. S., Occhipinti, M. L., Yang, Y.-Y., Majcherek, T., Haver, D., and Oki, L. (2017). Managing urban runoff in residential neighborhoods: nitrogen and phosphorus in lawn irrigation driven runoff. *PLoS One* 12:e0179151. doi: 10.1371/journal.pone.0179151

Trivedi, P., and Axe, L. (2000). Modeling Cd and Zn sorption to hydrous metal oxides. *Environ. Sci. Technol.* 34, 2215–2223. doi: 10.1021/es991110c

United States Environmental Protection Agency [EPA] (1994). *Method 200.2: Sample Preparation Procedure for Spectrochemical Determination of Total Recoverable Elements.* Washington, DC: US Environmental Protection Agency.

Walther, C., Büchner, S., Filella, M., and Chanudet, V. (2006). Probing particle size distributions in natural surface waters from 15 nm to 2 μm by a combination of LIBD and single-particle counting. *J. Coll. Interface Sci.* 301, 532–537. doi: 10.1016/j.jcis.2006.05.039

Xia, T., Kovochich, M., Liong, M., Madler, L., Gilbert, B., Shi, H., et al. (2008). Comparison of the mechanism of toxicity of zinc oxide and cerium oxide nanoparticles based on dissolution and oxidative stress properties. *ACS Nano* 2, 2121–2134. doi: 10.1021/nn800511k

Yang, Y., Vance, M., Tou, F., Tiwari, A., Liu, M., and Hochella, M. F. (2016). Nanoparticles in road dust from impervious urban surfaces: distribution, identification, and environmental implications. *Environ. Sci. Nano* 3, 534–544. doi: 10.1039/c6en00056h

Young, A., Kochenkov, V., McIntyre, J. K., Stark, J. D., and Coffin, A. B. (2018). Urban stormwater runoff negatively impacts lateral line development in larval zebrafish and salmon embryos. *Sci. Rep.* 8, 1–14.

Zheng, Y., Mutzner, L., Ort, C., Kaegi, R., and Gottschalk, F. (2019). Modelling engineered nanomaterials in wet-weather discharges. *NanoImpact* 16:100188. doi: 10.1016/j.impact.2019.100188

Zuo, X., Fu, D., and Li, H. (2012). Speciation distribution and mass balance of copper and zinc in urban rain, sediments, and road runoff. *Environ. Sci. Pollut. Res.* 19, 4042–4048. doi: 10.1007/s11356-012-0907-z